JOURNAL OF GUIDANCE, CONTROL, AND DYNAMICS
Vol. 30, No. 6, November–December 2007

Engineering Notes

ENGINEERING NOTES are short manuscripts describing new developments or important results of a preliminary nature. These Notes should not exceed 2500 words (where a figure or table counts as 200 words). Following informal review by the Editors, they may be published within a few months of the date of receipt. Style requirements are the same as for regular contributions (see inside back cover).

Low-Thrust Interplanetary Transfers, Including Escape and Capture Trajectories

Yang Gao*
Chinese Academy of Sciences,
100080 Beijing, People's Republic of China

DOI: 10.2514/1.26427

Introduction

OPTIMAL low-thrust interplanetary transfers in the heliocentric frame have been studied in many documented articles in which the planetary escape and capture maneuvers were not addressed. For example, [1–4] demonstrated different methods to find optimum steering programs for heliocentric orbital transfers. Moreover, a number of state-of-the-art low-thrust trajectory optimization tools are also available for mission designers. The Jet Propulsion Laboratory (JPL) developed the well-known SEPTOP and VARITOP [5] (SEPTOP's predecessor) programs that have been used for decades. More recently, JPL has demonstrated devotion to developing new low-thrust programs such as MYSTIC [6] and MALTO [7], which are more sophisticated and capable of designing complicated low-thrust trajectories. On the other hand, optimizing low-thrust planetocentric escape and capture trajectories has also been studied (see [8–11]). These prior efforts and studies reveal that mission designers are interested in low-thrust transfers from a low-Earth orbit (LEO) to a low-planet orbit. However, the literature dealing with optimizing the entire mission, including both heliocentric and planetocentric transfer trajectories, still appears to be somewhat limited. The most commonly used method is the patched-conic approximation, which was used by Melbourne and Sauer [12] in the 1960s. The interplanetary leg and planetocentric spirals are optimized separately and then patched together. Currently, this approximation method is still in wide use by mission designers.

In this Note, an approach is proposed to estimate the mission performances (e.g., flight time and propellant mass) of low-thrust interplanetary transfers, including escape and capture trajectories. During the escape or capture phases, the continuous tangential or antitangential thrust (null in shadow) is used and J_2 perturbations are considered. The low-thrust escape or capture spirals are computed by a fast algorithm (an analytic orbital averaging technique plus a short-duration integration process) that significantly reduces the trajectory propagation time. With the patched-conic approximation, the proposed approach makes it possible to formulate the entire low-thrust interplanetary transfer trajectory in a single nonlinear programming parameter optimization problem. It should be noted that the shadow conditions may significantly affect propellant consumption, flight time, and the ephemeris time that the capture or escape begins. The inclusion of shadowing distinguishes this work from most previous research.

The purpose of the proposed approach is not to generate high-fidelity trajectory solutions but to provide a preliminary analysis tool for mission designers to quickly estimate the mission performances of low-thrust interplanetary transfers that include escape and capture trajectories. The many-revolution planetocentric spiral trajectories in the presence of shadowing and J_2 perturbations are propagated using orbital averaging, which results in much fewer steps than precise numerical integration. The proposed approach is particularly useful for determining a particular mission's trend with respect to variations in system parameters. An optimal Earth–Mars transfer is obtained in this Note to provide an example. Furthermore, the preliminary solutions obtained with the proposed method could be used as good initial guesses for further trajectory optimization to generate high-fidelity solutions.

Analytic Orbital Averaging Technique

The majority of the orbital revolutions for the escape and capture trajectories are computed by an analytic orbital averaging technique (AOAT), illustrated in [13]. Computing the analytic incremental changes of the classical orbital elements (assuming tangentially directed low thrust) with respect to eccentric anomaly over an orbital arc is the key feature of the AOAT, which are summarized as follows (see [13] for details):

$$\int_{E_{ex}}^{E_{en}} \frac{da}{dE}\,dE = \frac{2a^3}{\mu} f_{in} \int_{E_{ex}}^{E_{en}} \sqrt{1-e^2\cos^2 E}\,dE \tag{1}$$

$$\int_{E_{ex}}^{E_{en}} \frac{de}{dE}dE = \frac{2a^2}{e\mu}(1-e^2) f_{in}\left\{\int_{E_{ex}}^{E_{en}}\left(\sqrt{1-e^2\cos^2 E} - \frac{1}{\sqrt{1-e^2\cos^2 E}}\right)dE + \left[\ell n\left(\sin E + \frac{1}{e}\sqrt{1-e^2\cos^2 E}\right)\right]_{E_{ex}}^{E_{en}}\right\} \tag{2}$$

$$\int_{E_{ex}}^{E_{en}} \frac{di}{dE}\,dE = \int_{E_{ex}}^{E_{en}} \frac{d\Omega}{dE}\,dE = 0 \tag{3}$$

$$\int_{E_{ex}}^{E_{en}} \frac{d\omega}{dE}\,dE = -\frac{2a^2}{e^2\mu}\sqrt{1-e^2} f_{in}[\sqrt{1-e^2\cos^2 E} + \sin^{-1}(e\cos E)]_{E_{ex}}^{E_{en}} \tag{4}$$

The two integrals in Eqs. (1) and (2) are approximated as

$$\int_{E_{ex}}^{E_{en}} \sqrt{1-e^2\cos^2 E}\,dE \approx [\sqrt{1-e^2}E + (1-\sqrt{1-e^2})(0.5E - 0.25\sin 2E)]_{E_{ex}}^{E_{en}} \tag{5}$$

Received 10 July 2006; revision received 2 July 2007; accepted for publication 5 July 2007.

*Associate Research Fellow, Academy of Opto-Electronics, Department of Space System Engineering, P.O. Box 8701; GaoY@aoe.ac.cn.

$$\int_{E_{ex}}^{E_{en}} \left(\sqrt{1-e^2\cos^2 E} - \frac{1}{\sqrt{1-e^2\cos^2 E}} \right) \mathrm{d}E \approx \frac{-e^2}{\sqrt{1-e^2}c} [0.5E + 0.25\sin 2E]_{E_{ex}}^{E_{en}} \tag{6}$$

where a, e, i, Ω, and ω are the first five classical orbital elements, and E is eccentric anomaly. The cylindrical shadow exit and entrance angles in eccentric anomaly are denoted by E_{ex} and E_{en}. The in-plane tangential acceleration's magnitude is f_{in} and its direction is aligned with the velocity direction. Note the parameter c ($c = 0.8$, see [13]) is a constant value for the approximation of Eq. (6). With the notation $\mathbf{x}_A = [a, e, i, \Omega, \omega]^T$ representing the averaged elements due to f_{in} and $\bar{\mathbf{x}} = [\bar{a}, \bar{e}, \bar{i}, \bar{\Omega}, \bar{\omega}]^T$ representing the averaged elements per orbit due to J_2 perturbations, the total incremental changes of the classical orbital elements per revolution are computed as

$$\Delta\mathbf{x} = \int_{E_{ex}}^{E_{en}} \frac{\mathrm{d}\mathbf{x}_A}{\mathrm{d}E}\,\mathrm{d}E + \frac{\mathrm{d}\bar{\mathbf{x}}}{\mathrm{d}t}\frac{2\pi}{n} \tag{7}$$

The mass loss Δm and flight time Δt per revolution are

$$\Delta m = -\frac{2\eta P}{(gI_{sp})^2}\left[\frac{1}{n}(E_{en} - e\sin E_{en} - E_{ex} + e\sin E_{ex})\right] \tag{8}$$

$$\Delta t = \frac{2\pi}{n} \tag{9}$$

where P is input power, I_{sp} is specific impulse, η is engine efficiency, g is sea-level Earth gravitational acceleration, and $n = \sqrt{\mu/a^3}$. With $\mathbf{y} = [\mathbf{x}\ \ t\ \ m]$ and $\Delta\mathbf{y} = [\Delta\mathbf{x}\ \ \Delta t\ \ \Delta m]$, the elements for the $(i+1)$th revolution are computed using the elements for the ith revolution.

$$\mathbf{y}_{i+1} = \mathbf{y}_i + \Delta\mathbf{y}_i \tag{10}$$

Determining the Number of Revolutions Before Escape

The results presented in [13] only demonstrate satisfactory approximations of the AOAT up to certain orbital energy levels, beyond which the AOAT is invalid. In fact, the orbital energy tends toward positive values and the eccentricity tends to increase quickly to unity during the final few orbital revolutions before escape. This characteristic obviously violates the basic assumption of the orbital averaging, which assumes that the incremental changes of semimajor axis and eccentricity per revolution are relatively small. Under the assumption that no shadow exists ($E_{ex} = 0$ and $E_{en} = 2\pi$) at high altitudes, the incremental changes of semimajor axis and eccentricity are

$$\int_0^{2\pi} \frac{\mathrm{d}a}{\mathrm{d}E}dE = \frac{2a^3}{\mu} f_{in}\pi(\sqrt{1-e^2} + 1) \tag{11}$$

$$\int_0^{2\pi} \frac{\mathrm{d}e}{\mathrm{d}E}dE = \frac{2a^2}{\mu}(1-e^2) f_{in}\frac{-e\pi}{\sqrt{1-e^2}c} \tag{12}$$

Equations (11) and (12) indicate that the AOAT results in the continuously increasing semimajor axis and decreasing eccentricity as $0 < e < 1$. If the semimajor axis is large enough, the eccentricity incremental change computed by Eq. (12) would be a large negative value, which might result in a negative value of eccentricity using Eq. (10). However, it is known that a negative value for eccentricity is not defined. In fact, the eccentricity should increase to unity quickly. Note that the undefined negative eccentricity is only caused by mathematic modeling of Eqs. (11) and (12), and this property is then used for justifying the escape condition. That is to say, if a negative (or nonpositive) value of eccentricity appears in the AOAT at a high altitude without the shadow effect, the escape condition is met. Therefore, the spacecraft escapes at the $(i+1)$th orbital revolution if

$$e(i+1) \le 0 \tag{13}$$

at a high altitude, and

$$E_{ex} = 0 \quad \text{and} \quad E_{en} = 2\pi \tag{14}$$

at the ith revolution.

Meanwhile, the number of orbital revolutions before escape is obtained as $m_{rev} = i$ by the AOAT. A preselected value (denoted by m_{bwd}) can be chosen to define how many revolutions would be propagated by alternative methods just before escape. Therefore, the AOAT is only valid for trajectory propagation from the first to the $(m_{rev} - m_{bwd})$th orbital revolution.

Trajectory Propagation with Respect to Orbital Energy

The final m_{bwd} orbital revolutions are propagated using a set of equinoctial elements p, f, g, and L, where $p = a(1-e^2)$, $f = e\cos(\omega)$, $g = e\sin(\omega)$, and $L = \omega + \theta$. Note that θ is defined as true anomaly. Derivatives of the equinoctial elements and time with respect to orbital energy are

$$\frac{\mathrm{d}p}{\mathrm{d}\varepsilon} = \frac{2p}{w}\sqrt{\frac{p}{\mu}} f_\theta \frac{1}{f_{in} v} \tag{15}$$

$$\frac{\mathrm{d}f}{\mathrm{d}\varepsilon} = \frac{1}{f_{in} v}\sqrt{\frac{p}{\mu}}\left[f_r \sin L + [(w+1)\cos L + f]\frac{f_\theta}{w}\right] \tag{16}$$

$$\frac{\mathrm{d}g}{\mathrm{d}\varepsilon} = \frac{1}{f_{in} v}\sqrt{\frac{p}{\mu}}\left[-f_r \cos L + [(w+1)\sin L + g]\frac{f_\theta}{w}\right] \tag{17}$$

$$\frac{\mathrm{d}L}{\mathrm{d}\varepsilon} = \frac{1}{f_{in} v}\sqrt{\mu p}\left(\frac{w}{p}\right)^2 \tag{18}$$

$$\frac{\mathrm{d}m}{\mathrm{d}\varepsilon} = -\frac{1}{f_{in} v}\frac{2\eta P}{(gI_{sp})^2} \tag{19}$$

$$\frac{\mathrm{d}t}{\mathrm{d}\varepsilon} = \frac{1}{f_{in} v} \tag{20}$$

where $w = 1 + f\cos L + g\sin L$, v is orbital velocity, and f_r and f_θ are radial and circumferential acceleration components. This set of equinoctial elements has no singularity when the orbit is parabolic or hyperbolic. The changes of i and Ω are not included because only the in-plane tangential thrust is employed and J_2 perturbations are neglected for propagation of the final m_{bwd} orbital revolutions. Note that no third-body perturbations are included. The integration variable is orbital energy, which ranges from a negative value (elliptical orbit) to a nonnegative value (parabolic or hyperbolic orbit). The initial energy ε_0 is determined by a at the $(m_{rev} - m_{bwd})$th revolution computed by the AOAT, and the final energy ε_f can be specified a priori. The values of a, e, and ω [the states at the $(m_{rev} - m_{bwd})$th revolution computed by the AOAT] are used to obtain initial values of the equinoctial elements $p(\varepsilon_0)$, $f(\varepsilon_0)$, and $g(\varepsilon_0)$. Note that $L(\varepsilon_0)$ is not given by the AOAT and can be a user-defined value or a variable to be optimized. Simple numerical integration methods (fixed-step, fourth-order Runge–Kutta method is employed in this Note) can be used to propagate the final m_{bwd} revolutions; 200 integration steps and $m_{bwd} = 5$ are chosen for numerical examples in this Note to achieve a good tradeoff between solution accuracy and computational load.

Some readers may not be convinced with regard to the need to precisely integrate the final extra m_{bwd} revolutions. The original idea is to use as few steps as possible for propagating long-duration spiral

Table 1 Initial orbits for escape simulation

Case	a_0, Earth radii	e_0	i_0, rad	Ω_0, rad	ω_0, rad	θ_0, rad	Escape energy, km^2/s^2
1	3.82	0.731	0.2	1	2	0	0
2	2.1	0.5	0.3	3	4	0	0
3	1.08	0.01	0.5	5	6	0	0

trajectories. Orbital averaging is used to propagate majority of revolutions, which is computationally much cheaper than precise integration. Because the final few revolutions (with rapidly increasing eccentricity) are difficult to model by either analytic means or orbital averaging, precise numerically integration must be used for this small portion of escape leg. Fortunately, the AOAT method easily computes the number of revolutions before escape, which then determines when to switch from orbital averaging to precise integration for the final m_{bwd} revolutions. In fact, the 200-step Runge–Kutta integration warrants the propagation accuracy and is not a computational burden in current PC computers.

Three cases are simulated to compare results obtained by the proposed approximate method and precise integration. Three types of initial orbits in Table 1 are cited from [13]. The spacecraft parameters are $P = 5$ kW, $I_{\text{sp}} = 3000$ s, and $\eta = 0.6$, and the initial mass is $m_0 = 1000$ kg. The calendar date is fixed at 1 January 2008 for all initial orbits (required for Earth-shadow conditions). Using a series of values of $L(\varepsilon_0)$ [$L(\varepsilon_0) = n\pi/4$ ($n = 0, 1, \ldots, 8$), prescribed at the $(m_{\text{rev}} - m_{\text{bwd}})$th revolution] from 0 to 2π, the trajectory propagation results show that the errors in propellant masses and flight times computed by precise integration and the proposed approximate method do not exceed 2%. The time histories of eccentricity are presented in Fig. 1, with the value of $L(\varepsilon_0)$ selected so that the approximate solutions closely match the precise integration solutions.

Once we obtain the final states at a predefined energy level (for example, $\varepsilon_f = 0$ is the minimum energy for escape), the final planetocentric states can be transformed into states expressed in the heliocentric frame for the patched-conic approximation.

Capture Trajectories Using Low Anti-Tangential Thrust

Computing capture trajectories is considered as the backward process for computing escape trajectories. The AOAT and the short-duration integration method are used to propagate trajectories backward from the final target orbit to the point at which $\varepsilon_0 = 0$ (i.e., zero relative velocity on the approach asymptote). Similarly, the total number of capture spiraling revolutions can be estimated by the AOAT. The first few capture revolutions (i.e., $m_{\text{bwd}} = 5$) are integrated backward using Eqs. (15–20). Note that the date, spacecraft mass, and orbital elements at the low orbit of the target planet should be given for backward trajectory propagation.

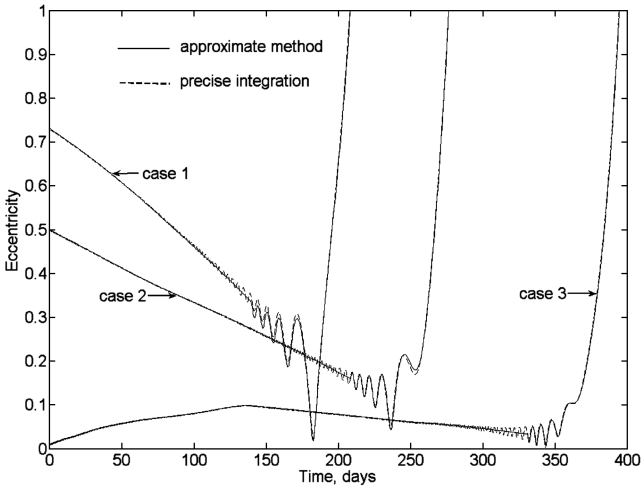

Fig. 1 Time histories of eccentricity.

Formulation of Interplanetary Transfers Including Escape and Capture Trajectories

Figure 2 illustrates a general interplanetary mission that includes escape and capture spiral trajectories, in which the spacecraft escapes planet 1 and spirals into planet 2. Note that m is the spacecraft mass and t is the date at specified time constants.

A parameter optimization problem is readily formulated, and the optimization variables are the planet-1 low-orbit departure date and $L(\varepsilon_0)$ in the planet-1-centered frame; optimal control parameters and transfer times in the heliocentric frame; and the planet-2 low-orbit arrival date, mass at the planet-2 low orbit, and $L(\varepsilon_f)$ in the planet-2-centered frame. The performance index (to be minimized) is total transfer time or propellant mass. In addition to the constraints for the dynamic equations in the heliocentric and planetocentric frames, there are some additional constraints:

$$m_f^{(\text{hel})} = m_0^{(\text{cap})} \tag{21}$$

$$t_f^{(\text{hel})} = t_0^{(\text{cap})} \tag{22}$$

$$\mathbf{x}_{s/c}^{(\text{hel})}\left(t_f^{(\text{hel})}\right) = \mathbf{x}_{P_2}^{(\text{hel})}\left(t_f^{(\text{hel})}\right) \tag{23}$$

where $\mathbf{x}$ denotes the position and velocity vector. Equations (21) and (22) imply that the time and mass are constrained to be equal at the patching point between the heliocentric and planet-2-centered frames. Equation (23) implies that the spacecraft's position and velocity are constrained by the target body's heliocentric position and velocity (i.e., capture energy $\varepsilon_0 = 0$). Equation (23) could be written as Eq. (24) strictly in terms of the classical patched-conic approximation.

$$\mathbf{x}_{s/c}^{(\text{hel})}\left(t_f^{(\text{hel})}\right) = \mathbf{x}_{P_2}^{(\text{hel})}\left(t_f^{(\text{hel})}\right) + \mathbf{x}_{s/c}^{(\text{cap})}\left(t_0^{(\text{cap})}\right) \tag{24}$$

In fact, $\mathbf{x}_{s/c}^{(\text{cap})}(t_0^{(\text{cap})})$, which is on the order of the planet-centered distance unit, is much smaller than $\mathbf{x}_{P_2}^{(\text{hel})}(t_f^{(\text{hel})})$, which is on the order of a heliocentric astronomic unit. Therefore, Eq. (23) is a loose and reasonable constraint for preliminary analysis and is helpful to improve the convergence robustness of optimization. Likewise, the initial condition for the heliocentric leg is given by the terminal condition of the escape spiral trajectory:

$$m_0^{(\text{hel})} = m_f^{(\text{esc})} \tag{25}$$

$$t_0^{(\text{hel})} = t_f^{(\text{esc})} \tag{26}$$

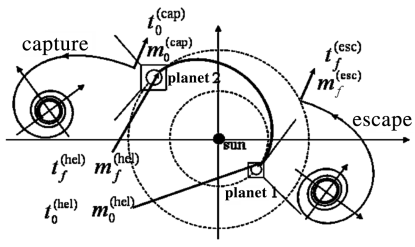

Fig. 2 Interplanetary missions including an escape and capture spiral trajectories.

Table 2 Solutions with different initial masses

Initial mass, kg	1500	1200	1000	800
Final mass, kg	883.30	711.15	594.17	473.47
LEO departure date	05/02/2008	08/16/2008	11/06/2008	01/04/2009
Earth-escape date	07/12/2009	08/06/2009	08/27/2009	08/20/2009
Mars-capture date	12/11/2010	11/20/2010	11/16/2010	10/25/2010
LMO arrival date	10/02/2011	08/01/2011	06/20/2011	04/10/2011
Escape rev./capture rev.	2108/1022	1737/968	1394/867	1107/672
Escape fuel/capture fuel, kg	315/100	251/80	209/66	166/53

$$\mathbf{x}_{s/c}^{(\mathrm{hel})}\left(t_0^{(\mathrm{hel})}\right) = \mathbf{x}_{P_1}^{(\mathrm{hel})}\left(t_0^{(\mathrm{hel})}\right) + \mathbf{x}_{s/c}^{(\mathrm{esc})}\left(t_f^{(\mathrm{esc})}\right) \quad \text{or} \quad \mathbf{x}_{s/c}^{(\mathrm{hel})}\left(t_0^{(\mathrm{hel})}\right) = \mathbf{x}_{P_1}^{(\mathrm{hel})}\left(t_0^{(\mathrm{hel})}\right) \tag{27}$$

A logical procedure to design the mission is stated as follows. First, the heliocentric transfer phase can be solved using many existing approaches; second, the AOAT is employed to predict the transfer time and propellant mass of escape and capture spiral trajectories; third, based on the predicted transfer time and propellant mass for escape and capture spirals, the entire transfer trajectory is patched together and then optimized in a single optimization problem using the results obtained from the first and second steps.

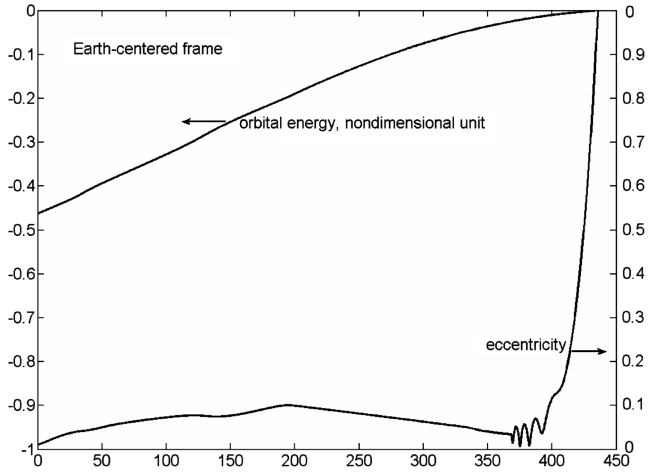

Fig. 3 Orbital energy and eccentricity in the Earth-centered frame.

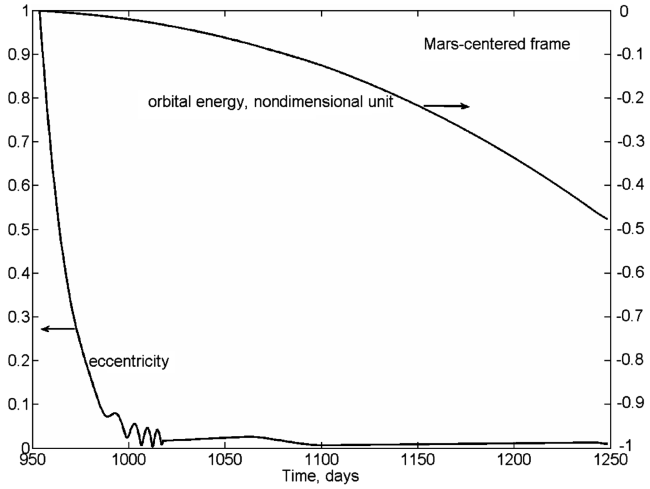

Fig. 4 Orbital energy and eccentricity in the Mars-centered frame.

Earth–Mars Trajectories, Including Earth Escape and Mars Capture

The proposed method is demonstrated by an Earth–Mars transfer using solar electric propulsion (SEP) that includes both Earth-escape and Mars-capture spiral trajectories. The SEP input power at 1 AU is $P_0 = 6.5$ kW, the specific impulse is $I_{\mathrm{sp}} = 3100$ s, and the thruster efficiency is $\eta = 0.65$. For the interplanetary transfer phase, the input power follows the inverse square law $P = P_0/r^2$, where r (in astronomical units) is the distance from the spacecraft to the sun. For simplicity, P is 6.5 kW for the Earth-escape phase and P is 2.8134 kW for the Mars-capture phase. The initial thrust-to-weight ratio of $2\eta P/(m_0 g^2 I_{\mathrm{sp}})$ is 1.8895×10^{-5} for the Earth-escape phase if the initial mass is $m_0 = 1500$ kg, and the thrust-to-weight ratio is much lower for the Mars-capture phase. The parameters for the initial LEO are $a = 1.08R_e$ (R_e is Earth radii), $e = 0.01$, $i = 28.5$ deg, $\Omega = 0$, and $\omega = 0$, and the parameters for the desired low-Mars orbit (LMO) are $a = 1.05R_m$ (R_m is Mars radii), $e = 0.01$, $i = 90$ deg, $\Omega = 0$, and $\omega = 0$. The shadow and J_2 perturbations in both Earth- and Mars-centered frames are included. The obliquity angle (angle between the planet equatorial plane and the ecliptic plane) of Earth and Mars are set to 23.4 and 24 deg, respectively. Note the shadowing geometry is primarily determined by the departure date, which gives the direction of the sun, initial spacecraft orbital plane, and initial ascending node. The JPL planetary ephemerides [14] are used for the optimization of the Earth–Mars transfer. The interplanetary transfer phase is solved using a hybrid method [15] in which the costate variables are used to govern the optimal control and a typical burn-coast-burn engine sequence is assumed.

The minimum-fuel solutions are summarized in Table 2 for cases with different initial masses, which is helpful to mission designers for determining trends of other mission parameters with the varying initial spacecraft mass. It is shown that both escape and capture phases involve large numbers of orbital revolutions. The time histories of orbital energy and eccentricity for the case of 1500-kg initial mass are shown in Figs. 3 and 4. All preliminary solutions obtained by the proposed method are good initial guesses for further optimization to generate high-fidelity trajectories.

Conclusions

A new approach was developed for optimizing key mission indices (such as flight time and propellant mass) for low-thrust interplanetary transfers that include the effects of escape and capture trajectories. The many-revolution, long-duration spiral trajectories in the respective planetocentric frames are computed by an analytic orbital averaging technique and a short-duration precise integration process with respect to orbital energy (planetary shadow and J_2 perturbation effects are also considered). The inclusion of shadowing effects on the mission optimization problem is a main contribution of this work. The complete transfer trajectory is modeled using multiple body-centered frames and a simple patched-conic approach, and the optimal mission design problem is solved as a single optimization problem. Several optimal Earth–Mars missions are obtained to demonstrate that the proposed approach is simple, quick, and robust and useful for mission trade studies with respect to varying mission parameters.

References

[1] Betts, J. T., "Optimal Interplanetary Orbit Transfers by Direct Transcription," *Journal of the Astronautical Sciences*, Vol. 42, No. 3, 1994, pp. 247–268.

[2] Kluever, C. A., "Optimal Low-thrust Interplanetary Trajectories by Direct Method Techniques," *Journal of the Astronautical Sciences*, Vol. 45, No. 3, 1997, pp. 247–262.

[3] Tang, S., and Conway, B. A., "Optimization of Low-Thrust Interplanetary Trajectories Using Collocation and Nonlinear Programming," *Journal of Guidance, Control, and Dynamics*, Vol. 18, No. 3, 1995, pp. 599–604.

[4] Coverstone, C. V., and William, S. N., "Optimal Low-Thrust Trajectories Using Differential Inclusion Concept," *Journal of the Astronautical Sciences*, Vol. 42, No. 4, 1994, pp. 379–393.

[5] Williams, S. N., "An Introduction to the Use of VARITOP—A General Purpose Low-Thrust Trajectory Optimization Program," Jet Propulsion Laboratory, JPL D-11475, Pasadena, CA, 24 Jan. 1994.

[6] Whiffen, G. J., and Sims, J. A., "Application of a Novel Optimal Control Algorithm to Low-Thrust Trajectory Optimization," AAS/AIAA Space Flight Mechanics Meeting, Santa Barbara, CA, American Astronautical Society, Paper 01-209, 11–15 Feb. 2001.

[7] Sims, J., Finlayson, P., Rinderle, E., Vavrina, M., and Kowalkowski, T., "Implementation of a Low-Thrust Trajectory Optimization Algorithm for Preliminary Design," AAS/AIAA Astrodynamics Specialist Conference and Exhibit, Keystone, CO, AIAA Paper 2006-6746, Aug. 2006.

[8] La Mantia, M., and Casalino, L., "Optimization of Low-Thrust Capture and Escape Trajectories," 41st AIAA/ASME/SAE/ASEE Joint Propulsion Conference and Exhibit, Tucson, AZ, AIAA Paper 2005-4266, 10–13 July 2005.

[9] Kluever, C. A., "Optimal Earth-Capture Trajectories Using Electric Propulsion," *Journal of Guidance, Control, and Dynamics*, Vol. 25, No. 3, 2002, pp. 604–606.

[10] Petropoulos, A., Whiffen, G., and Sims, J., "Simple Control Laws for Continuous-Thrust Escape and Capture and Their Use in Optimization," AIAA/AAS Astrodynamics Specialist Conference, Monterey, CA, AIAA Paper 2002-4900, 5–8 Aug. 2002.

[11] Ranieri, C. L., and Ocampo, C. A., "Indirect Optimization of Spiral Trajectories," *Journal of Guidance, Control, and Dynamics*, Vol. 29, No. 6, 2006, pp. 1360–1366.
doi:10.2514/1.19539

[12] Melbourne, W. G., and Sauer, C. G., Jr., "Performance Computations with Pieced Solutions of Planetocentric and Heliocentric Trajectories for Low-Thrust Missions," *JPL Space Programs Summary*, No. 37–36, Vol. 4, Jet Propulsion Lab., Pasadena, CA, 31 Dec. 1965, pp. 14–19.

[13] Gao, Y., and Kluever, C. A., "Analytic Orbital Averaging Technique for Computing Tangential-Thrust Trajectories," *Journal of Guidance, Control, and Dynamics*, Vol. 28, No. 6, 2005, pp. 1320–1323.

[14] Standish, E. M., "The JPL Planetary and Lunary Ephemerides DE402/LE402," *Bulletin of the American Astronomical Society*, Vol. 27, 1995, p. 1203.

[15] Gao, Y., and Kluever, C. A., "Low-Thrust Interplanetary Orbit Transfers Using Hybrid Trajectory Optimization Method with Multiple Shooting," AIAA/AAS Astrodynamics Specialist Conference and Exhibit, Providence, RI, AIAA Paper 2004-5088, 16–19 Aug. 2004.